CFD characterisation of the gyroid lattice structure

Introduction

I Gyroid definition
1) Lattices structures
2) Mathematical model
3) Mechanical properties

II CFD Methodology
1) Methodology of the study
2) CFD set up

III Validation
1) Test rig and test sample
2) Cylinder study
3) Gyroid study

IV Roughness modelling
1) Roughness effect
2) CT-scan
3) Roughness modelling in OpenFoam

V Unit Cell level simulation for model development
1) Methodology
2) CFD set up
3) Results
4) Model

Conclusion

Introduction

There is a growing interest in understanding the mechanical and thermal properties of minimal surface lattice structures produced with additive manufacturing. This study focuses on the gyroid minimal surface as shown in Figure 1 below.

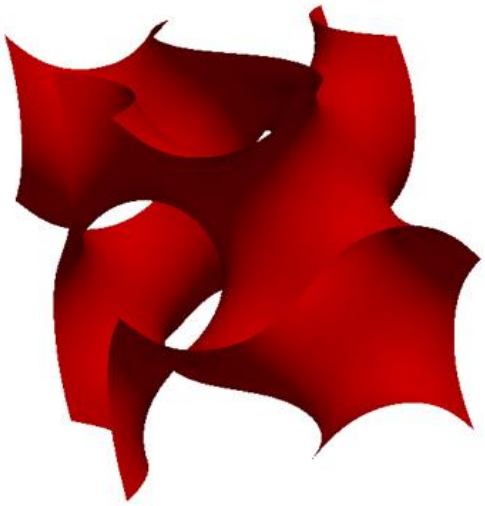

Figure 1: Gyroid Unit Cell

This surface represents the interface between the fluid and the solid. Whilst the mechanical properties of these lattices have been extensively studied for lightweight applications in aerospace and defence sectors, their thermal behaviour is not well investigated. In order to expand their use for thermal application, for example in compact heat exchangers, the heat transfer and flow through the gyroid needs to be investigated. The objective of this work is to develop a model for pressure drop and heat transfer of the flow through gyroid unit cell lattice as a function of the Reynolds number.

I Gyroid definition

1) Lattice structures

Lattice structures are an attractive class of materials with a mathematically defined internal structure and exhibiting specific properties of great interest in engineering. A significant body of research into the structure and properties of the cellular structures observed in the nature has organised with Gibson and Ashby in 1997. The cellular lattice is defined by a connected network of struts and the advantage of these lattices structures is to create stiff, strong load-bearing structures using as little material as possible or to be as light as possible.

The lattice materials are engineering lattices at small scale, their unit cells sizes are of the order of the millimeter or micrometer. This small scale allows the lattice material to be view both as a structure and as a material. They can be analyzed as a structure with conventional mechanical method at the unit cell scale but also as a material with its own set of global properties such as stiffness, strength thermal conductivity and diffusivity, electrical resistivity…. The lattice material can be used for several applications such as lightweighting, energy management, thermal insulation, filtration etc.

The development of additive manufacturing (AM) and specifically of Selective Laser Melting (SLM) allows the manufacturing of complex open periodic cellular structure with controlled porosity. The geometry of the lattices structures is variable and only some of them are self-supported, therefore adapted to SLM. One of them is the Gyroid lattice structure and some of their variant that have been extensively studied for lightweighting application in the aerospace and defense sector. So forth there is a growing interest in understanding the properties of these lattices produced with SLM.

2) Mathematic definition

The Gyroid surface belongs to the family of structures known as triple periodic minimal surfaces (TPMS). These are minimal surfaces periodic in three independent directions, extending infinitely and, in the absence of self-intersections, partitioning the space into two separated volumes. This surface can be used to represent the interface between a solid and a fluid, and forms a lattice structure. Figure 2 represents example of TPMS and Figure 3 lattices structures build from them.

Figure 2: Dimensional tessellations of Schwarz's Primitive (left), and Diamond (centre) and Schoen's Gyroid (right) Triply Periodic Minimal Surfaces

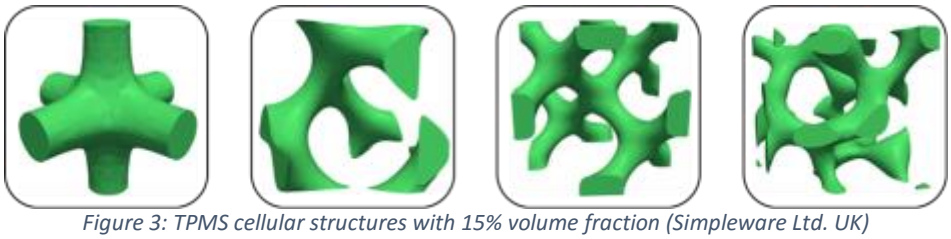

Figure 3: TPMS cellular structures with 15% volume fraction (Simpleware Ltd. UK)

In three-dimensional Cartesian coordinates x, y, z, the gyroid minimal surface is defined by the equation:

$$\sin\left(\frac{2\pi}{L}x\right)\cos\left(\frac{2\pi}{L}y\right)+\sin\left(\frac{2\pi}{L}y\right)\cos\left(\frac{2\pi}{L}z\right)+\sin\left(\frac{2\pi}{L}z\right)=t \qquad (1.1)$$

where L is the size of the cube, or the unit cell size, and t controls the volume fraction. Equation 1.1 demonstrates that the parameter t determines the type of the resultant lattice structure. The possible types are:

- t = 0, the gyroid surface divides the space in two regions with each a volume fraction of 50%.
- 0 < | t | < 1.1413, when | t | increases, the volume fraction decreases. To determine the desired volume fraction.
- t = 1.1413, the gyroid is at its minority network.
- 1.1413 < | t | < 1.5, the gyroid is no longer connected.
- | t | >1.5, the gyroid disappears.

To determine the desired volume fraction (VF), an approximation of the relationship between the volume fraction in function of t exists:

$$VF=\frac{(101.5-68.1*t)}{2}$$

From this definition, the Gyroid lattice surface can be constructed and therefore it is possible to study its properties as functions of several parameters such as the cell size and volume fraction.

3) Mechanical properties

The mechanical properties of the lattices structures depend on the properties of the material, the relative density (density of the lattice/density of the solid) and the topology of the lattice. For the lattices structures manufactured with AM, the build chamber, laser settings and morphology of the powder could also affect the quality of the lattices.

The gyroid geometry with a connectivity of three struts per joint is bending-domitated. As material, the gyroid lattices structures are interesting for their low stiffness and strength, and the large strains they can accommodate. These properties are attractive for cushioning, packaging, energy absorption and accommodating thermal shock.

A significant amount of research has already been undertaken into the structure and mechanical properties of these materials; however, their fluid flow and heat transfer characteristics have not been thoroughly investigated. This work will study the pressure drop and heat transfer of the flow through gyroid unit cell lattice as a function of the Reynolds number and the Volume Fraction.

II Methodology

1) Methodology of the study

The study is originally split in three parts, the first part consists in validating the CFD set up, the second part in modelling a scan of the manufacture geometry and the last part is the CFD modelling at the unit cell level to develop a model for heat transfer and pressure drop.

- The validation consists in doing some CFD simulation on the test sample to compare the results with the tests. This study consists in using the CAD file for the manufacturing and to mesh it. Then the simulation is done with OpenFoam and the results of the CFD are compared to the experimental one.

- The manufactured part are scanned with a μ-CT scan. The original CAD file is compared with the scanned part and the discrepancies analysed as well as their impact on the pressure drop and heat transfer.

- The CFD modelling at the unit cell level takes advantage of the periodic boundary conditions to reduce the mesh size and run a significant number of simulations. The two parameters varying are the volume fraction and the Reynolds number, after possessing sufficient results from the simulations, we purpose to develop a model for pressure drop and heat transfer. This model can later on be implemented to model a large number of lattices as a porous media.

2) CFD set up

The flow is assumed to be incompressible and steady. A constant temperature boundary condition is applied to the walls in accordance to the experimental set up. Then the appropriate OpenFoam (Open Foam v.2.3.0) solver for our set up is buoyantBoussinesqSimpleFoam with the gravity set to 0. To reproduce the experimental conditions, the inlet temperature is fixed to 298K and the wall temperature to 363K. Moreover, the inlet velocity is fixed to match the various experimental points and the k-Omega SST turbulence model is applied for the turbulent cases.

III Validation

1) Experimental set up

The samples were manufactured from AlSi10Mg using a Renishaw AM250 SLM machine. The laser power, laser scan speed and hatch spacing were 200 W, 600 mm/s and 150 µm. The dimensions of the sample are 11mm x 9 mm x 90 mm. The test rig, developed at HiETA Technologies, is composed of two heating walls at the top and bottom of the sample. The heating walls are heated electrically at four points each to 363K using an AC power supply to maintain a uniform surface temperature. Air was directed at ambient temperature into the channels. A flowmeter was utilized to measure the air- flow rate in the system. The inlet and outlet bulk temperatures were measured using two thermocouples located at the entry and the exit of the test duct.

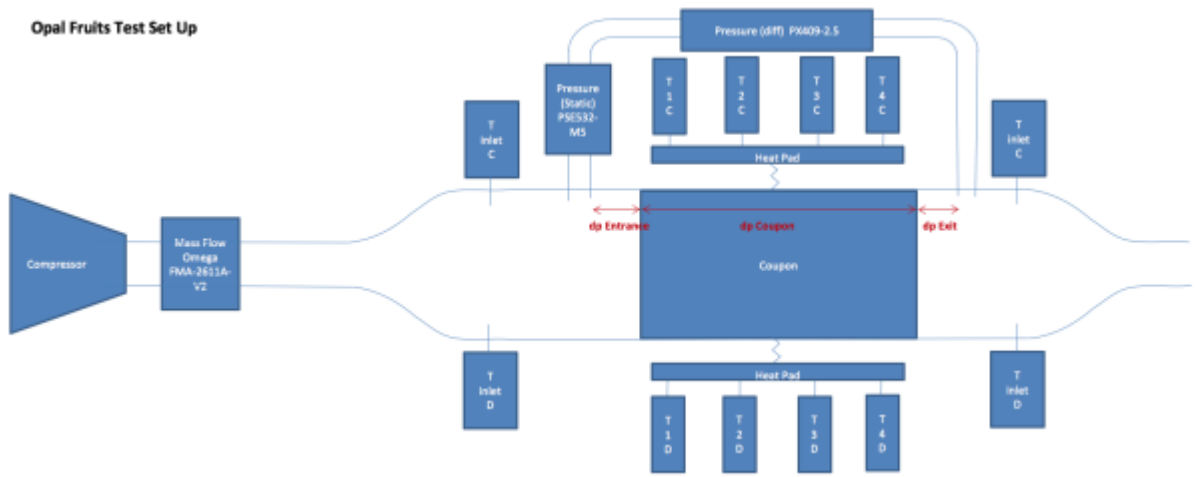

Figure 4: Opal Fruits Test Set up

The lattice tested is the Gyroid of 4mm cell size and 30% of volume fraction. The test piece dimensions are 11 mm x 9 mm x 90 mm as you can see in the picture below. This sample was tested for the Reynolds of 900, 1800 and 2400.

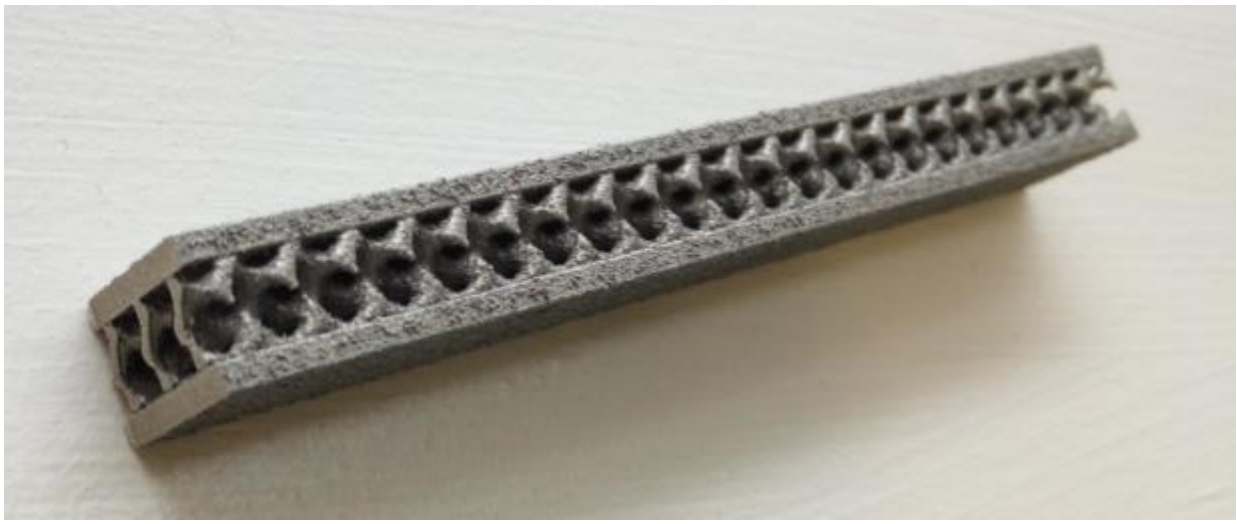

Figure 5: Test sample of the Gyroid 4mm cell size, 30% of Volume fraction.

2) Cylinder study

To help to interpret the test results for the gyroid test sample, a similar study was done for a simpler geometry, a cylindrical channel. The cylinder's dimensions are adapted to the test rig with a diameter of 3 mm and a length of 90 mm. Three pipes were built in the test sample. For this case the experimental results were compared to the CFD and empirical correlations for pressure drop and heat transfer. Several Reynolds were modelled to cover different flow regimes.

The CFD set up is similar than the one described in II 2). The cases were run with 2nd order numerical schemes.

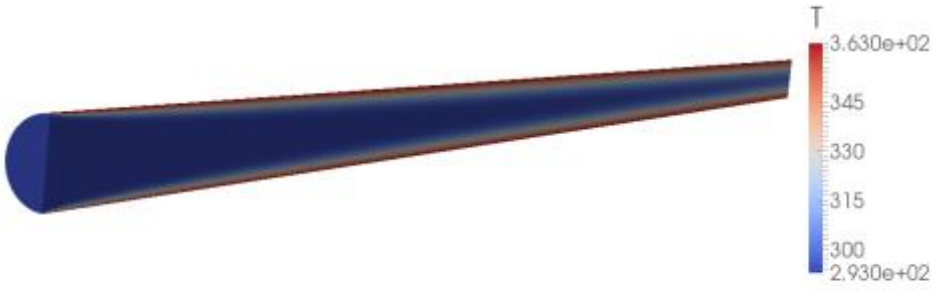

Figure 6: Temperature along the cylindrical channel for the Reynolds number 800.

Empirical correlations for the friction factor in laminar and turbulent flow in circular channels were used to compare the theoretical value of the friction factor with that from the experiments and simulations. For the transitional regime between turbulent and laminar, an average of the two correlations is used.

Re <2300 $$f = \frac{64}{Re} \quad (3.1)$$

Re >10000 $$f = \frac{1}{[0.790 \ln(Re) - 1.64]^2} \quad (3.2)$$

Equations 3.3 and 3.4 describe the empirical correlations for the Nusselt number in laminar and turbulent flow. An average is used for transition flow as well but in that case the correlation for the turbulent flow is valid for lower Reynolds numbers than with the friction factor correlation.

Re <2300 $$Nu = 3.66 + \frac{0.065 Re Pr \frac{D}{L}}{1 + 0.04 \left(Re\, Pr \frac{D}{L} \right)^{2/3}} \quad (3.3)$$

Re >4000 $$Nu = \frac{\left(\frac{f}{8}\right)(Re - 1{,}000) Pr}{1 + 12.7 \left(\frac{f}{8}\right)^{1/2} \left(Pr^{2/3} - 1\right)} \quad (3.4)$$

For each simulation point, a corresponding experimental test was performed. The experimental, simulation and empirical results for the friction factor and the Nusselt number are presented in Figure 7. The errors of the experimental cases being very low, the error bars are not shown in the graph. The error for the Nusselt number is less than 0.5% and for the friction factor less than 3%.

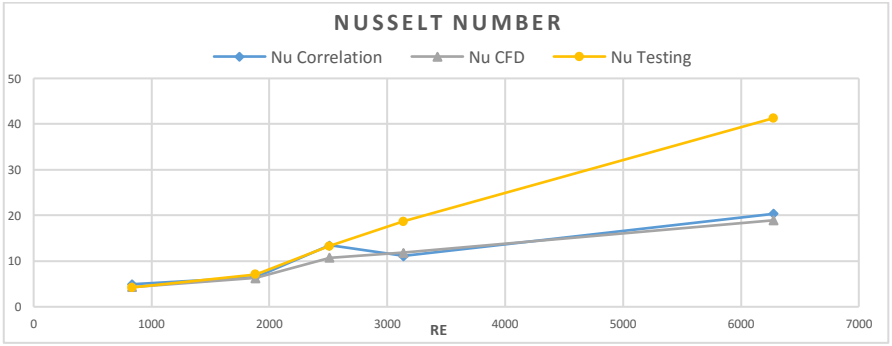

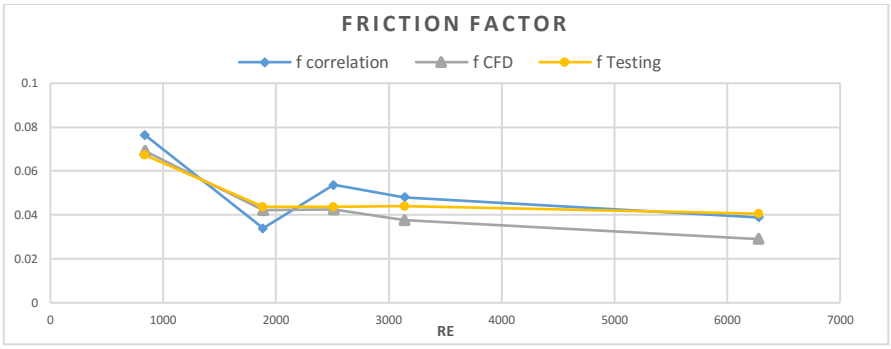

Figure 7: Comparison of the correlation, CFD and experiment in cylindrical channel for the Nusselt number and the friction factor

The results for Nusselt number are consistent between the CFD and the empirical correlations. The friction factor shows some discrepancies for turbulent flow but this can be explained by inaccuracies in the empirical correlations being used. Indeed, this particular range of Reynolds numbers represents the gap between the two regimes of the equations 3.1 and 3.2, and in this region, an average between the laminar and turbulent correlation is used. On the other hand, the experimental results differ significantly for the Nusselt number when the flow reaches the turbulent regime while for the friction factor the results stay globally consistent. The experimental friction factor value is slightly above the CFD but this might be attributed to the inherent surface roughness of the part. The reasons for the difference between the CFD and the experimental results need to be further investigated.

3) Gyroid test sample modelling

For the simulation of the Gyroid test sample, the STL used for manufacturing was provided for the modelling. The CAD file is shown in Figure 8 below.

Figure 8: Stl file used to build the Gyroid test sample

The first attempt was to mesh the STL file with Pointwise but the poor quality of the file made it very challenging. Therefore, as shown below we use snappyHexMesh. The mesh process with this tool is limited, and we used an alternative tool Avizoo. Avizo is an image-based meshing tool which handle easily STL files. It is then possible to improve the surface mesh significantly and to generate good quality tetrahedral elements for the fluid's volume.

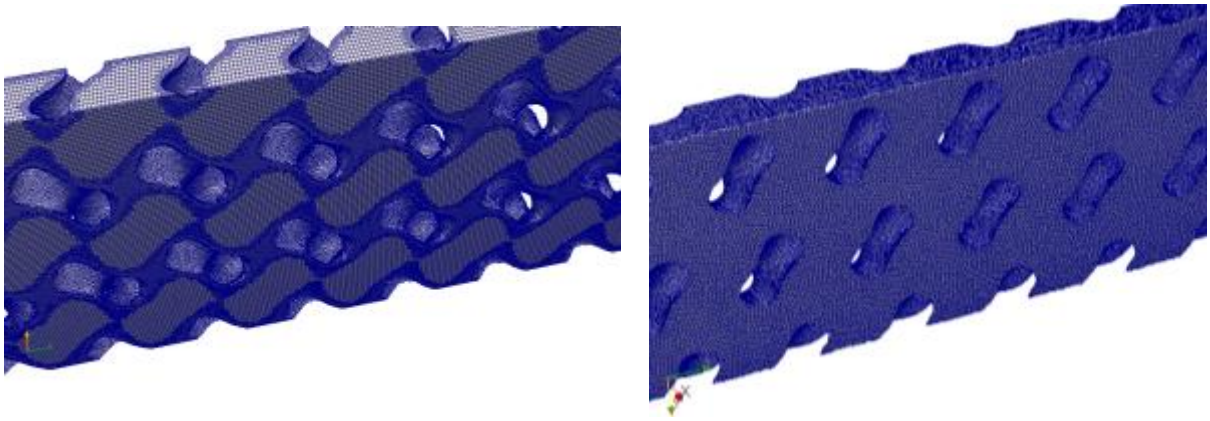

Figure 9: Mesh generated with snappyHexMesh (on the left) and with Avizo (on the right)

Once the geometry is meshed, the calculation was run using the setup described before. But the instability of the flow prevented to get 2nd order for the numerical scheme despite remeshing with the software Avizoo. Thus the case has been run with transient modelling for the lower Reynolds number.

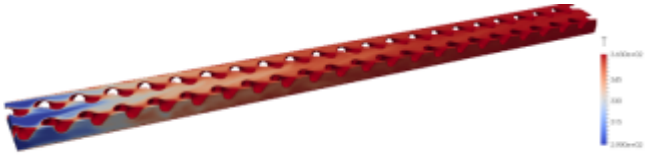

Figure 10: Evolution of the temperature inside the test sample for Re=900.

The results with the mesh generated with snappyHexMesh are shown in Figure 11 for the Nusselt number and for the friction factor. The temperature distribution is also presented in the Figure 10 for a Reynolds number of 900. The errors for the experimental case are less than 0.6% for the Nusselt number and the error bars are shown in the graph for the friction factor. The graph for the Nusselt number shows very similar results for the CFD and the experimental results. On the other hand, the friction factor is significantly higher for the experimental results than for the CFD, which is consistent with the previous study and can be again explained by the roughness of the part.
It is worth noting that the outlet temperature reached the wall temperature for the two cases with higher Reynolds number. This explains the results for the Nusselt number.

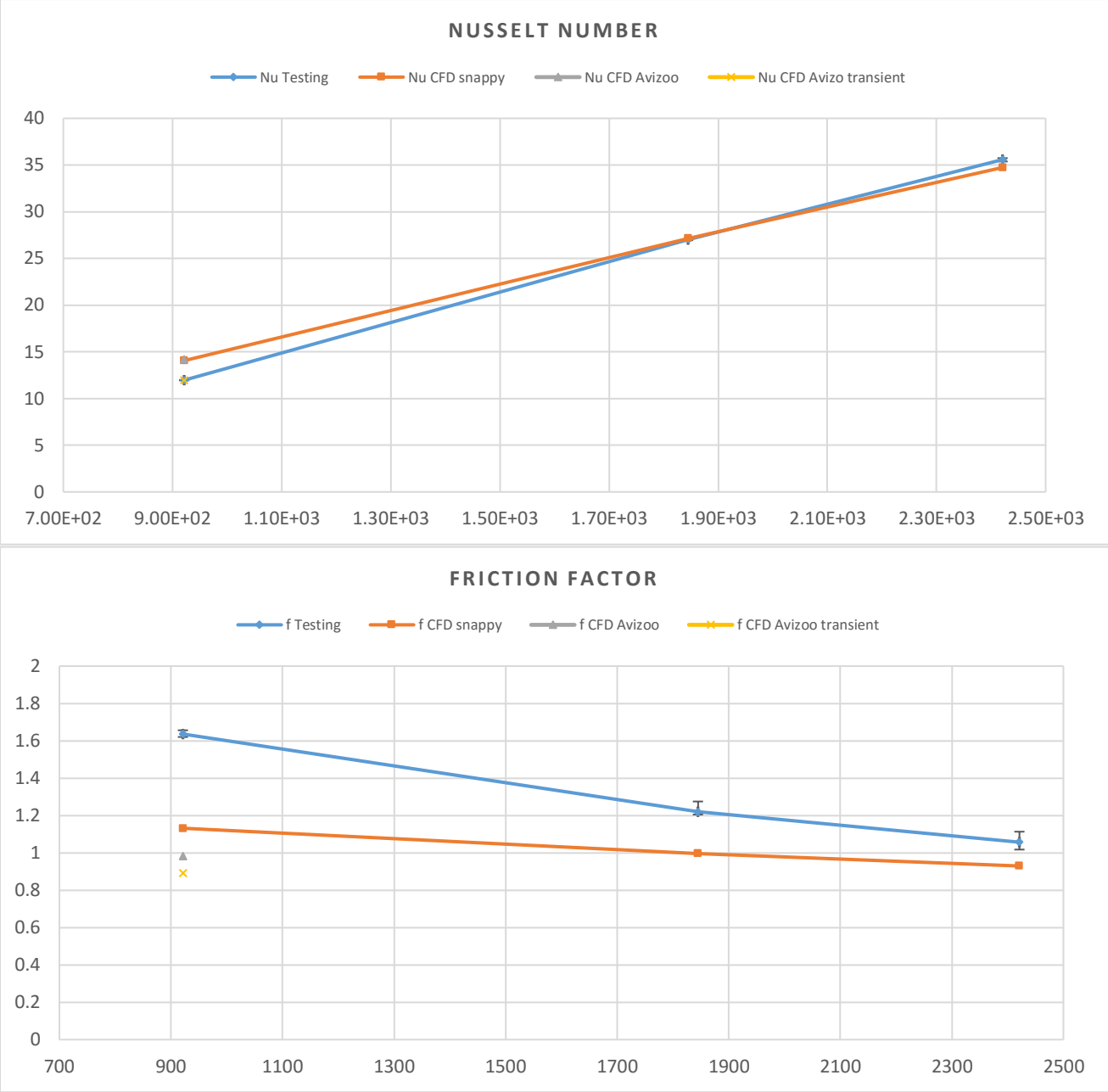

Figure 11: Comparison of CFD and experiment in gyroid test sample for the Nusselt number and the friction factor

IV Roughness modelling

1) Roughness effect

In regards of the discrepancies between the experimental and modelling results, further work is required. As it could be explained by the effect of the roughness of the part, we are going to investigate the effect of the roughness on the results.

Empirical correlations for the friction factor in turbulent flow in circular channels were used to compare the theoretical value of the friction factor and Nusselt number with several roughness values and the previous results.

For Re > 4000:

Colebrook–White equation $$\frac{1}{\sqrt{f}} = -2log\left(\frac{\varepsilon}{3.7D_h} + \frac{2.51}{Re\sqrt{f}}\right)$$

There are several explicit approximation solutions to this equation. And the Haaland equation was chosen to calculate the friction factor.

Haaland equation $$\frac{1}{\sqrt{f}} = -1.8log\left(\left(\frac{\varepsilon/D}{3.7}\right)^{1.11} + \frac{6.9}{Re}\right)$$

The Nusselt number is then calculated from the friction factor using the same correlation than in the previous study. The exact value of the surface roughness being unknown so far, the correlations are plotted for the roughness values of 10, 20 and 40 µm.

Figure 12: Comparison of the correlation including surface roughness, CFD and experiment in cylindrical channel for the Nusselt number and the friction factor

We can see that the effect of the roughness on the Nusselt number and friction factor is consistent with the discrepancies observed in the previous study. Therefore, a test sample for the cylinder have been manufactured and drilled to get smooth pipes. The experiments on the sample will be performed as soon as possible.

2) CT-scan

Some μ-CT scans have been performed in the University of Exeter on four test samples. Two test samples were scanned for the cylindrical channels with the two and three pipes. Then the gyroid 4mm of cell size and 30% of volume fraction and the gyroid 3mm cell size and 30% of volume fraction were scanned as well. A portion of the sample with the three cylinders have been scanned to increase the resolution and analyse the surface roughness more accurately.

Our study focused mainly on this last scan. To capture the detail of the roughness of the part, a very high resolution is needed.
The image –based processing software Avizoo is used to analyse the data from the scan. The portion of the scan is duplicated several times to reproduce a cylinder of the same length than the test sample as shown in Figure 13.

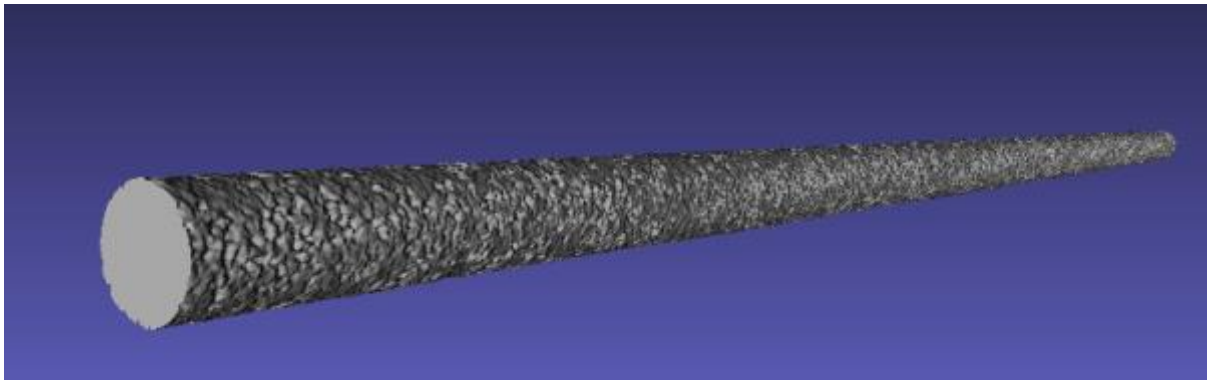

Figure 13: Scan of a cylindrical channel built with AM.

After analysing the scan, it seems that the roughness is significant in the part. The software Avizoo allows to generate a mesh of the surface. A detailed mesh is firstly generated to capture the surface in details.

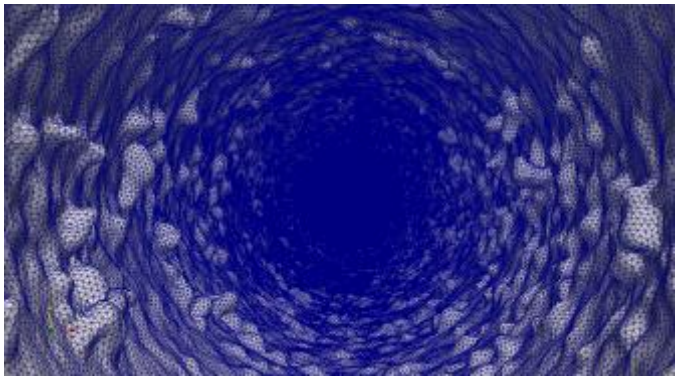

Figure 14: Detailed mesh of the inside of the as-built cylindrical channel.

This surface mesh is exported as a .stl file. The volume mesh is then generated with snappyHexMesh. With snappyHexMesh two mesh were generated, 3 and 5 million cells.

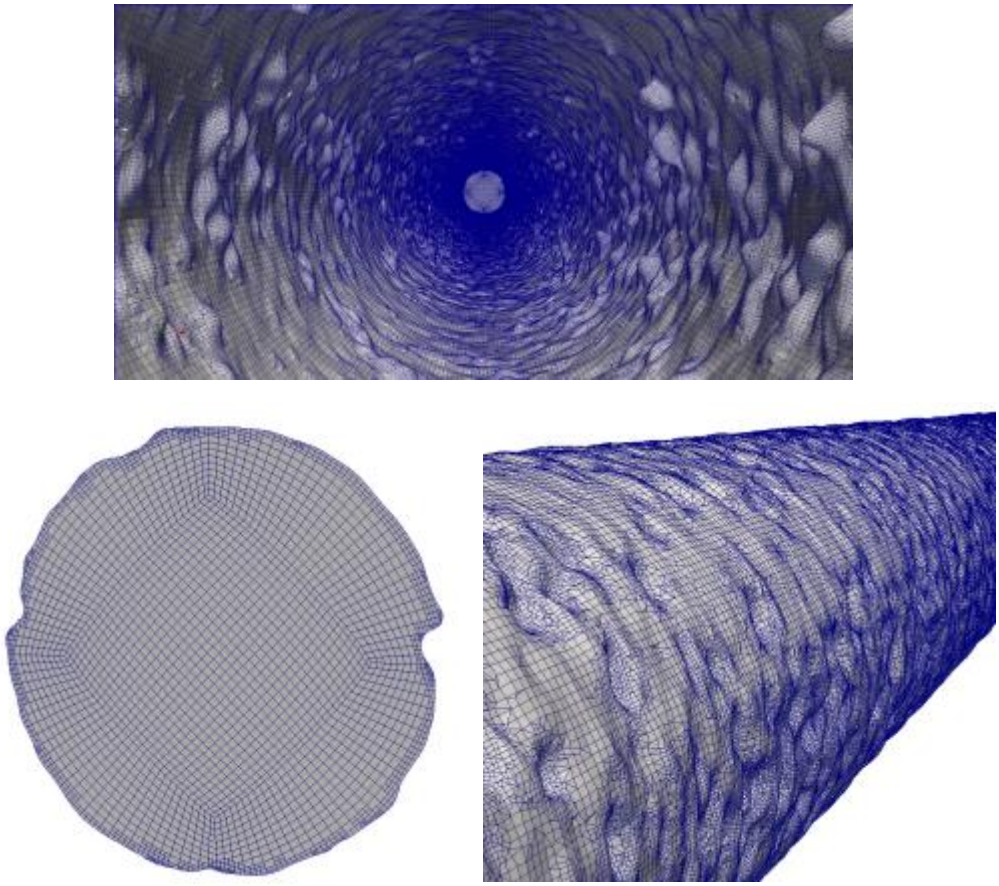

Figure 15: Mesh of 5 million cells generated with snappyHexMesh

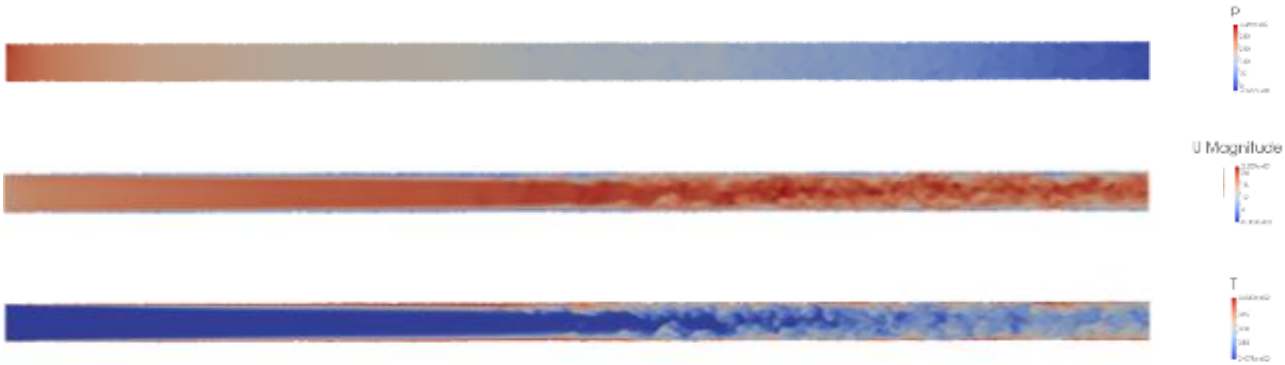

Figure 16: CFD result for the Pressure, Velocity and Temperature along the channel for Re=3000.

Figure 17: CFD results on the CT-scan geometry for Re= 800 ns Re=3000 with the mesh generated with snappyHexMesh

The results on the CT scan show an increase in the pressure drop and Nusselt number which consistent with the effect of the pressure drop. However, the results remain significantly different from the experimental results. The simulation need to be validated with a mesh sensitivity study. To have better control of the mesh, Avizoo was also used to generate a quarter cylinder. The surface mesh was coarsened to get a 9 milions cells quarter.

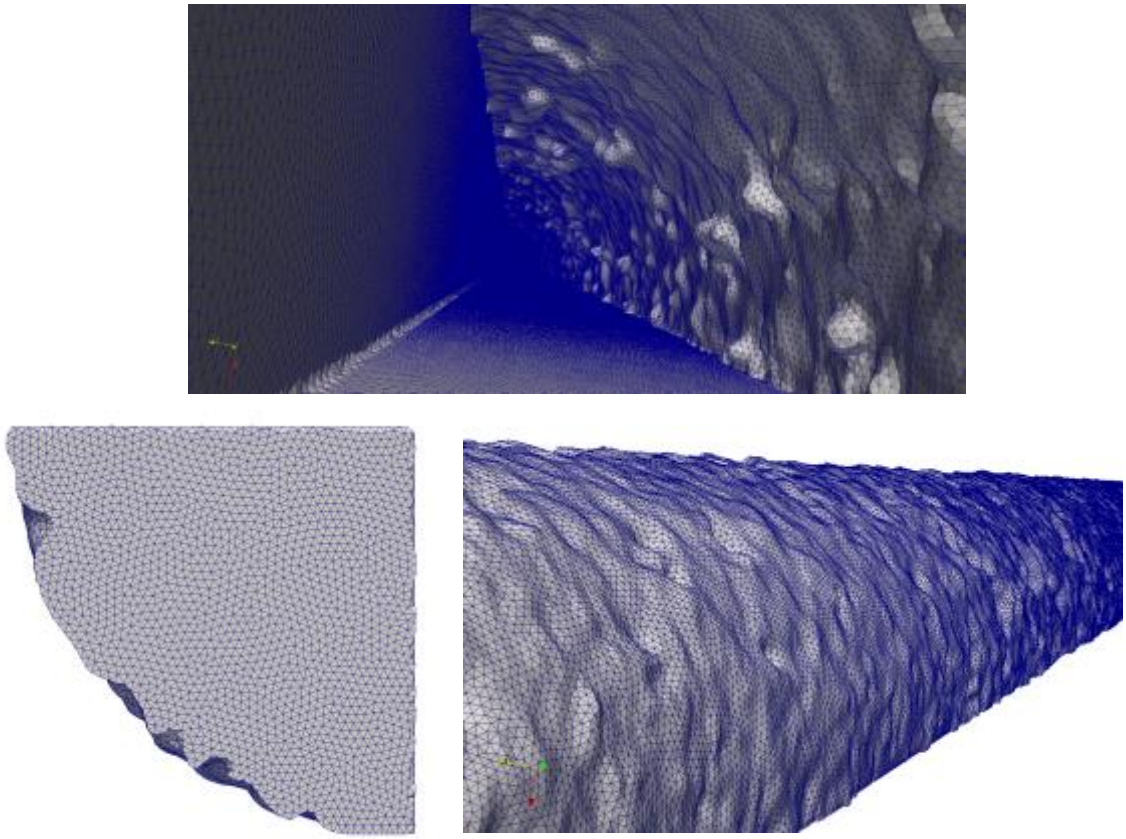

Figure 18: Mesh of the CT scan of the cylindrical channel generated with the software Avizoo

The simulation for the two Reynolds number 800 and 3000 are running with this mesh.

3) Roughness modelling in OpenFoam

An alternative to the CT-scan is the modelling of the roughness in the CFD in the wall functions. The wall functions being used only in turbulent modelling; we are focusing on the case with the higher Reynolds number of the study. Nevertheless, to use the wall function is valid only for a y+ value of at least 30, which sets the wall mesh size. The wall functions being used only in turbulent modelling; we are focusing on the cylindrical channel case with the higher Reynolds number of the study. To use the wall function, at a given Reynolds number, the mesh size at the wall needs to be in a certain range. But for the higher Reynolds number of our study, the mesh at the wall is relatively coarse. The interest being to capture what's happening in the wall, the mesh size makes it irrelevant. The CFD results without all functions and finer mesh at the wall is compared to a smooth turbulent model using the wall functions.

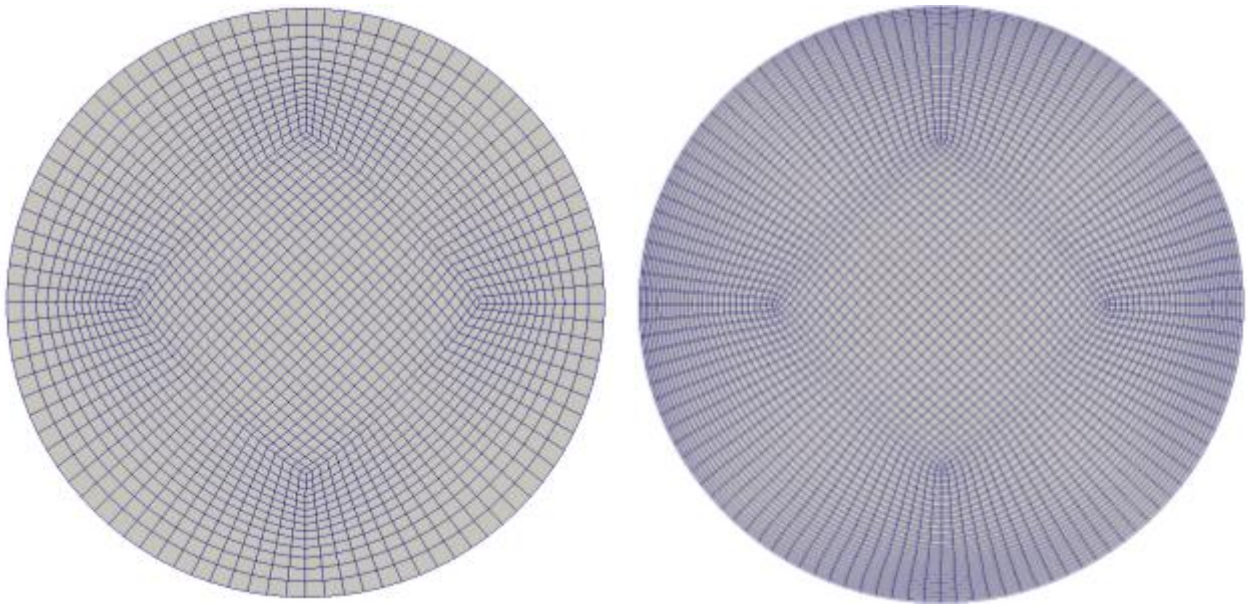

Figure 19:Mesh for the cylindrical channel. On the left, mesh constrained using the wall function. On the right, refined mesh to solve the boundary layer without the use of the wall function.

	Outlet temperature	Pressure drop
Fine Mesh	322.6918684	621.5879963
Coarse Mesh	341.5164347	586.0450625

Table 1: Comparison of the results with and without using the wall function

The results show a significance difference with invalidate the use of the wall function at low Reynolds number.

V Unit Cell level simulation for model development

1) Methodology

The cyclic boundary conditions are applied to reduce the mesh size and save computational time. Nevertheless, several unit cell are modelled in the flow direction to capture the entrance effects. The Reynolds number range covered is from 50 to 5000 determined by the heat exchanger application.

The first step is to choose one volume fraction and perform some CFD simulation for several Re. The functions J=f(Re) and ΔP=f(Re) are plotted and modelled. Then this study is reproduced for other volume fractions to develop a two models: J=f(Re,VF) and ΔP=f(Re, VF). This 1D model will be useful for 1D modelling of Heat Exchangers and to simulate a big group of unit cells as a porous media.

2) CFD set up

The CFD set is identical with the previous ones. The unit cell modelled in the flow direction should be long enough for the flow to develop which depends on the Reynolds number. To make sure the flow is developed, the flow parameters are sampled at the same point of the unit cell for each of them and plotted. Once the velocity is constant over the flow length, we can assume the flow is developed. Then we can extract the pressure drop and the heat transfer for a single unit cell.

3) Results

A preliminary study has been performed for the volume fraction of 30% at the unit cell level ignoring the surface roughness effect. The utility sample have been used to see the make sure the flow is developed in the model.

The gyroid geometry generating an unstable flow, the CFD model only converged at Steady state for the first order numerical scheme. We then got a fast trend curve.

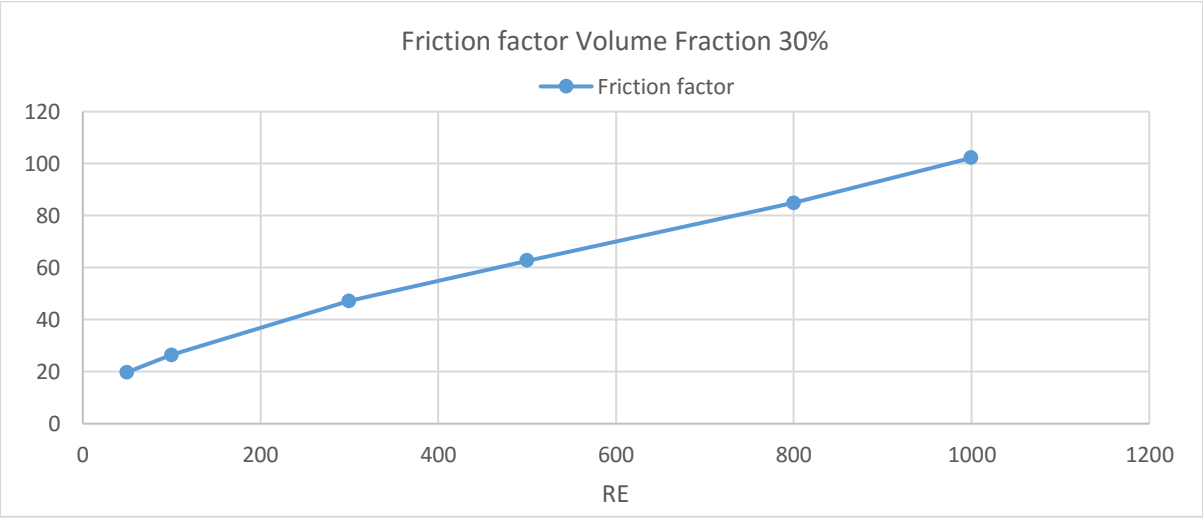

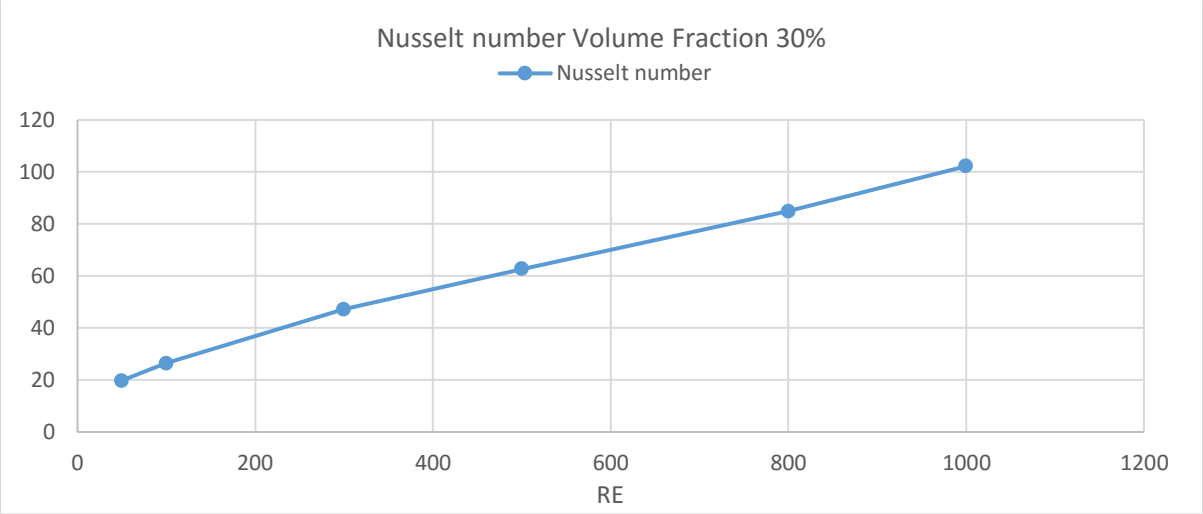

Figure 20:Friction factor and Nusselt number for the gyroid unit cell 30% of volume fraction and 4mmcell size.

For better accuracy, the modelling has been extended to run with second order numerical scheme in time. For very low Reynolds number, convergence with steady state could be achieved. But as we increased the Reynolds number, transient simulation was required.
The first Reynolds number have been modelled and the results are plotted below.

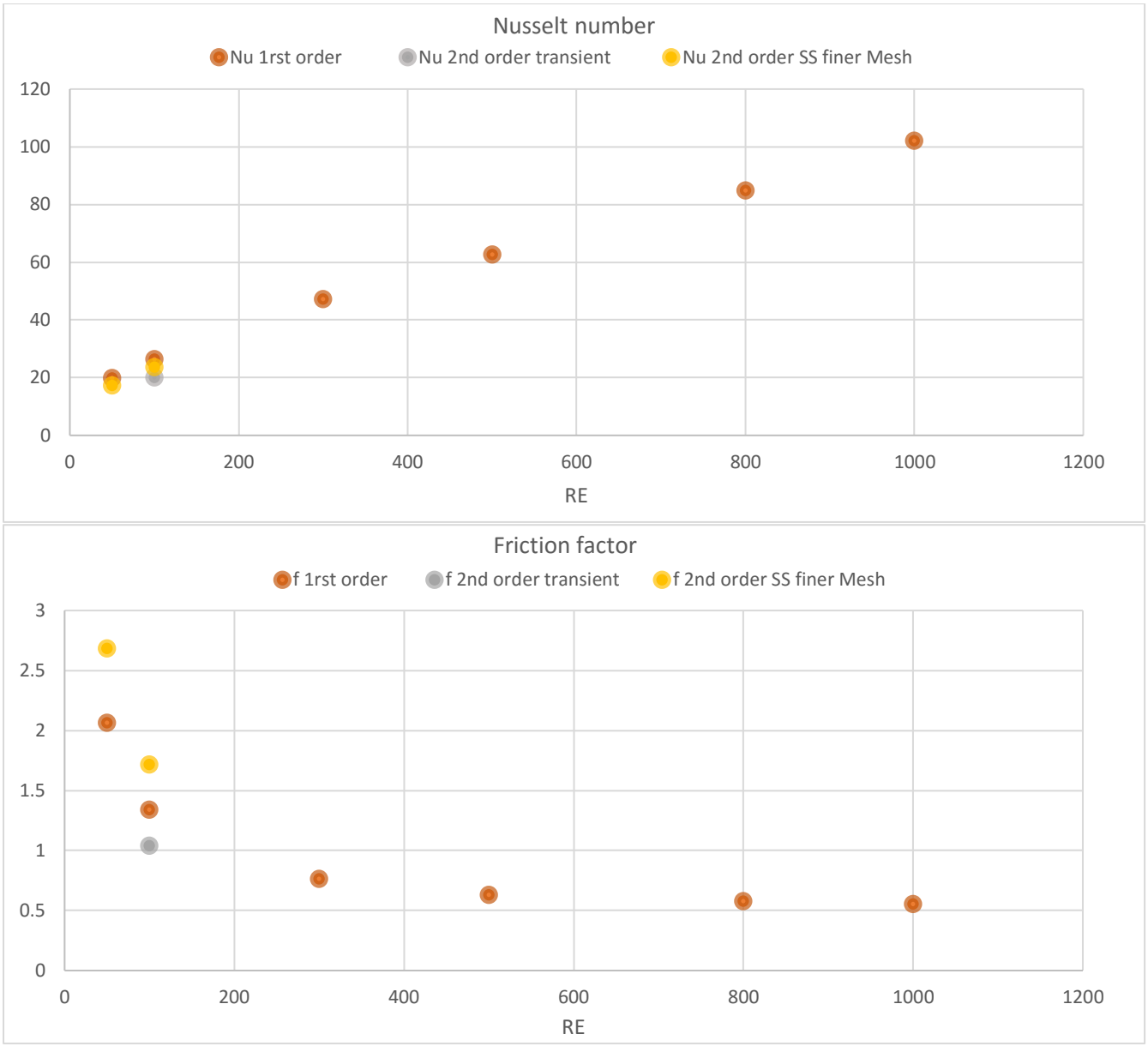

Figure 21: Comparison of the results with different CFD set up for the friction factor and the Nusselt number.

Reference:

Ashby M F (2006), The properties of foams and lattices.

Aremu A O, Maskery I, Tuck C, Ashcroft I A, Wildman R D, and Hague R I M (2014), A comparative finite element study of cubic unit cells for selective laser melting.

Hussein A Y (2013), The Development of Lightweight Cellular Structures for Metal Additive Manufacturing.

Khaseri S N, Deshpande V S, Fleck N A, The stiffness and strength of the gyroid lattice